ARTICLE

Check for updates

Ocean mass, sterodynamic effects, and vertical land motion largely explain US coast relative sea level rise

T. C. Harvey [1], B. D. Hamlington [2✉], T. Frederikse [2], R. S. Nerem[1], C. G. Piecuch[3], W. C. Hammond[4], G. Blewitt [4], P. R. Thompson[5], D. P. S. Bekaert[2], F. W. Landerer [2], J. T. Reager [2], R. E. Kopp [6], H. Chandanpurkar [2], I. Fenty [2], D. Trossman[7], J. S. Walker [6] & C. Boening[2]

Regional sea-level changes are caused by several physical processes that vary both in space and time. As a result of these processes, large regional departures from the long-term rate of global mean sea-level rise can occur. Identifying and understanding these processes at particular locations is the first step toward generating reliable projections and assisting in improved decision making. Here we quantify to what degree contemporary ocean mass change, sterodynamic effects, and vertical land motion influence sea-level rise observed by tide-gauge locations around the contiguous U.S. from 1993 to 2018. We are able to explain tide gauge-observed relative sea-level trends at 47 of 55 sampled locations. Locations where we cannot explain observed trends are potentially indicative of shortcomings in our coastal sea-level observational network or estimates of uncertainty.

[1] Smead Aerospace Engineering Sciences, Colorado Center for Astrodynamics Research, University of Colorado, Boulder, CO, USA. [2] Jet Propulsion Laboratory, California Institute of Technology, Pasadena, CA, USA. [3] Woods Hole Oceanographic Institution, Woods Hole, MA, USA. [4] University of Nevada Reno, Reno, NV, USA. [5] University of Hawaii at Manoa, Honolulu, HI, USA. [6] Institute of Earth, Ocean, and Atmospheric Sciences, Rutgers University, New Brunswick, NJ, USA. [7] University of Texas, Austin, TX, USA. ✉email: bhamling@jpl.nasa.gov

Changes in global mean sea-level (GMSL) provide an important measure of the warming climate[1–3], but regional relative sea-level (RSL) is most relevant for planners and decision-makers[4,5]. Since no process that affects sea-level causes a globally uniform sea-level change, regional sea-level changes usually differ from GMSL rise. Over the modern satellite era (1993-present) regional rates of geocentric sea-level (GSL) (i.e., sea-level relative to a reference geoid) can be more than double that of the GMSL in some locations while being near zero at other locations[6–8]. Local vertical land motion (VLM) adds to these deviations from the global mean[9–13]. Projections of future regional RSL changes typically rely on a thorough understanding of the underlying processes and how they contribute to sea-level change on differing temporal and spatial scales[14,15]. However, the diversity of these processes, the temporal and spatial scales over which they vary, and the available observations of individual processes make such a process-based assessment challenging.

The coastlines of the U.S. provide a particularly good example of the regional variability of recent RSL changes. During the modern altimeter era both tide gauges and altimetry observe a faster sea-level rise along the U.S. East coast than along the West coast (Fig. 1). In addition, there are local variations in the rate of RSL along each coastline. Many studies have investigated recent sea-level trends along coastlines of the U.S. and found that the high rates along the U.S. East coast have been associated with VLM and glacial isostatic adjustment[16–18], as well as ocean sterodynamic processes, with different processes acting North and South of Cape Hatteras where the Gulf Stream separates from the coast[19–24]. The highest rates of RSL rise in the continental U.S. are found in the western Gulf of Mexico, driven in large part by high rates of subsidence associated with subsurface fluid withdrawal (e.g.,[25]). In contrast to elevated rates seen along the Atlantic and Gulf coasts, the Pacific coast of the U.S. has seen rates lower than the global average during the satellite-altimeter era (e.g.,[26–28]). Decadal climate variability that is partly represented by the Pacific Decadal Oscillation (PDO) has played a role in suppressing recent RSL rise along this coastline over the satellite era, although similar decadal variability has also led to periods of substantially higher rates of rise over the course of the 20th century[29–31].

Understanding of the processes contributing to RSL along the U.S. coastlines has improved in recent years due partly to the maintenance and expansion of the sea-level observing network over this time period. Despite this rich era of observations, gaps or limitations in our understanding persist (e.g.,[32]) that impact our ability to provide assessments of future RSL[14]. In this study, we attempt to explain the RSL trends observed along U.S. coastlines during the satellite-altimeter era by accounting for and combining contributions from individual processes. Specifically, we investigate whether observed VLM, sterodynamic effects, and

ocean mass changes can explain local sea-level changes over 1993–2018 at 55 tide-gauge locations around the contiguous U.S. (Fig. 1). The goal of this work is to understand whether the identified processes fully account for RSL trends measured by tide gauges. We estimate the contributions of the different drivers of RSL rise and compare their sum to the observed sea-level trends over 1993–2018. Similar local sea-level budget exercises have been performed for some parts of the U.S. coastline and for different periods (e.g.,[16,18,33,34]). Our focus here is on the satellite-altimeter time period and the entirety of the coastal U.S. By only covering the time period from 1993 to 2018, the satellite-altimeter data provides an additional check on our process-based understanding. In cases where the budget "closes", there may be increased confidence that sea-level reconstructions and projections are accounting for the relevant processes, as this demonstrates a more complete understanding of why sea-level is changing. For locations where the process contributions do not match the observed RSL trends, we attempt to identify where our understanding is lacking and how this might be connected to the available observations.

Results

Drivers of regional relative sea-level change. For the assessment of sea-level at location r, we compare regional RSL trends (RSL_{TG}) to the effects of contemporary mass redistribution (CMR), sterodynamic effects (SD), glacial isostatic adjustment (GIA), and VLM. The difference between RSL_{TG} and the sum of these components gives a residual (RES), which, along with its uncertainties, we use as an indicator for our ability to fully explain observed RSL trends. We write the relationship between these terms using the following budget equation:

$$RSL_{TG}(r) = CMR(r) + SD(r) + GIA_{RSL}(r) \\ - (VLM(r) - GIA_{VLM}(r)) + RES(r) \tag{1}$$

GIA causes both sea-level changes and VLM, and therefore we separate these components to avoid double-counting:

$$GIA_{RSL}(r) = GIA_{GSL}(r) - GIA_{VLM}(r). \tag{2}$$

CMR is the GSL trend associated with contemporary mass redistribution resulting from changes in land ice mass and terrestrial water storage (Fig. 2a). SD is the trend in sterodynamic sea-level (see Gregory et al.[35] for extended definition) that encompasses both global-mean steric changes and regional sea-level changes associated with ocean dynamics (Fig. 2b). GIA_{RSL} is the RSL trend associated with glacial isostatic adjustment that encompasses both the effects on GSL (GIA_{GSL}, Fig. S1b) and VLM (GIA_{VLM}, Fig. 3a). VLM is the VLM trend observed by GPS (Fig. 3b). Since VLM encompasses the VLM associated with GIA, we subtract GIA_{VLM} from VLM in Eq. 1 to avoid counting this contribution twice, and the difference between the two is shown in Fig. 3c. Subsidence is defined as negative VLM, and leads to a positive contribution to RSL. We correct RSL_{TG} for the inverted barometer effect, which only has a small effect on the trends (see Fig. S1a and the Methods Section). We evaluate all quantities over 1993 to 2018. For altimetry-derived GSL trends (GSL_{ALT}), Eq. 1 reduces to the contemporary mass redistribution, sterodynamic variability, GIA, and residual terms:

$$GSL_{ALT}(r) = CMR(r) + SD(r) + GIA_{GSL}(r) + RES(r) \tag{3}$$

Fig. 1 Satellite-altimetry sea level trends. Observed sea-level trends (1993–2018) along the US coast. The map shows geocentric sea-level from satellite altimetry, and the individual dots relative sea-level trends measured by tide gauges.

By evaluating Eqs. 1, 3 along the coastlines of the U.S. with adequate attention to the uncertainty in the relevant processes, we assess our ability to explain recent RSL trends and the degree to which these limitations impact our understanding of them.
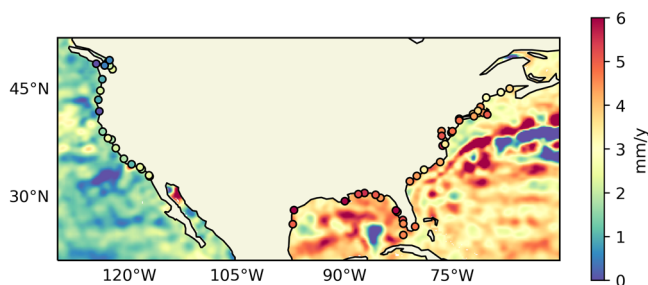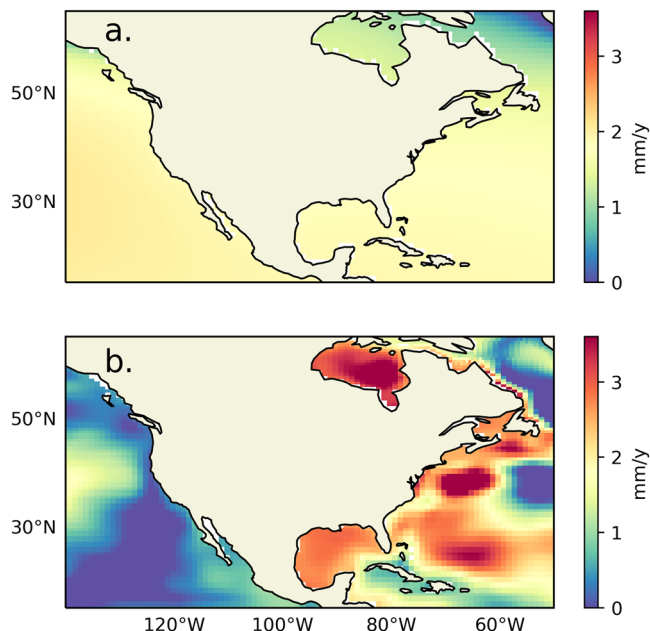
Fig. 2 Contributions to sea level trends. Estimated sea-level trends (1993–2018) due to (**a**) contemporary mass redistribution and (**b**) sterodynamic effects.
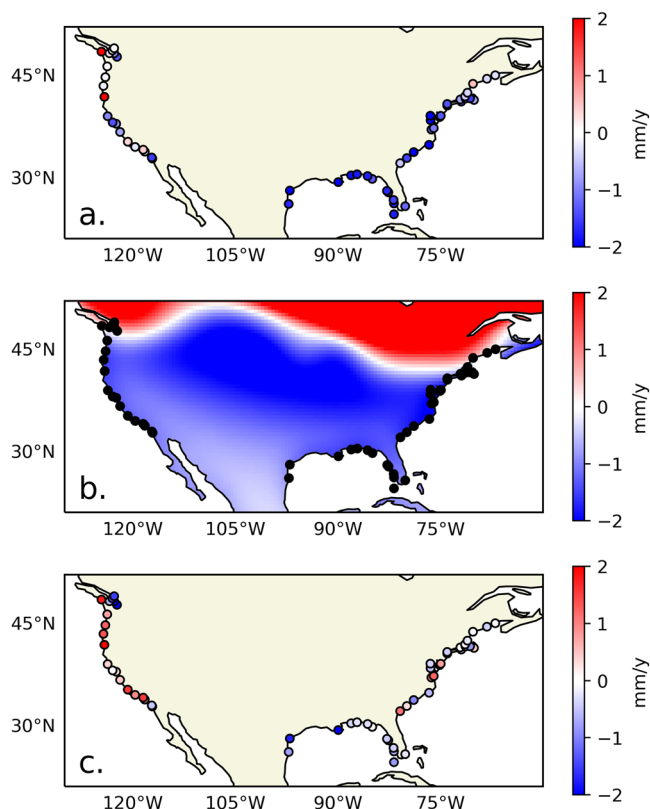

Fig. 3 Vertical land motion trends. Estimates of VLM at each tide-gauge location. **a** VLM estimated from GPS observations. **b** VLM associated with GIA. **c** VLM observed by GPS with the GIA contribution subtracted.

Contemporary mass redistribution. Due to gravitation, rotation, and deformation (GRD) effects, exchange of water mass between land and ocean, such as melting of glaciers and ice sheets or changes to the hydrological cycle, results in sea-level changes that vary from place to place[36–38]. In general, mass loss causes sea-

level to drop near the source of the loss, to rise at a reduced rate compared to the global average at intermediate distances from the source, and to rise at a rate exceeding the global average at larger distances from the source.

Here, we use the GRD patterns from Frederikse et al.[39] (Fig. 2a) who computed mass changes and the GRD response from four sources: The Antarctic Ice Sheet, Greenland Ice Sheet, glaciers, and land hydrology (which includes groundwater withdrawal, dam retention and natural water storage variability). The global-mean contribution from these four processes is 1.97 ± 0.35 mm/y over 1993–2018 (90% CI). Ice mass loss from the Antarctic ice sheet causes a roughly uniform trend along the coastlines of the U.S., while ice mass loss from Greenland and Arctic glaciers leads to a gradient along the U.S. east coast with increasing RSL trend contributions from north to south. Along the Pacific coast of the U.S., ice mass loss from the Alaskan glaciers leads to a similar north–south gradient.

Sterodynamic sea level variability. The sterodynamic contribution cannot be observed directly: from hydrographic observations, including Argo profiling floats, steric changes can be computed, but because sterodynamic effects also contain bottom pressure changes, especially on continental shelves, steric changes alone cannot be used to estimate the sterodynamic signal[32,40]. In terms of satellite observations, the footprint of satellite altimeters, uncertainty in the corrections applied to the data[41], and coarse resolution of the GRACE satellites[42] further inhibit the assessment of coastal trends. To estimate the sterodynamic contribution, we use the Estimating the Circulation & Climate of the Ocean[43] framework. ECCO is a data-constrained ocean circulation model that has been used for a wide range of investigations into sterodynamic sea-level across different timescales (e.g.,[44–46]). Figure 2b depicts the spatial pattern of the sterodynamic sea-level trends around the U.S., showing the different regimes along both coastlines with trends on the order of 2 mm/yr along the East coast, while the trends along the West coast are substantially smaller and often close to zero.

Glacial isostatic adjustment and vertical land motion. Vertical movement of land plays a key role in local RSL changes at many locations, including along U.S. coastlines[9–13,17,25,47]. One process that causes substantial VLM along the U.S. coastlines is glacial isostatic adjustment (GIA)[35,48], which is the ongoing solid-Earth response to the retreat of ice sheets after the last ice age. The impact of GIA on coastal VLM is especially noteworthy along the U.S. East Coast, where the ongoing collapse of the peripheral forebulge causes subsidence and aggravated rates of RSL rise[18,49–51]. To assess the GIA contribution at each tide gauge, we use the ensemble of GIA models from Caron et al.[52]. In addition to GIA, works such as Burgette et al.[53] have shown that inter-seismic strain associated with tectonic activity can cause uplift of up to several millimeters per year along parts of the western U.S. coastline. Apart from large-scale patterns of land motion due to GIA and tectonics, VLM occurs on much smaller spatial scales[54,55]. Compaction of sediments due to subsurface fluid extraction is an important driver of these local VLM patterns. Subsidence related to groundwater withdrawal can be especially pronounced in river deltas with large populations and extensive agriculture (e.g.,[56–60]). These effects are visible along the Gulf Coast[25] and Atlantic coast[61], with subsidence rates of up to several millimeters per year.

To estimate VLM unrelated to GIA, we use Global Positioning System (GPS) observations. GPS-based trend estimates to assess VLM at tide gauges have been used extensively in recent studies (*Woppelmann and Marcos*, 2016[62–64]). Many GPS records are
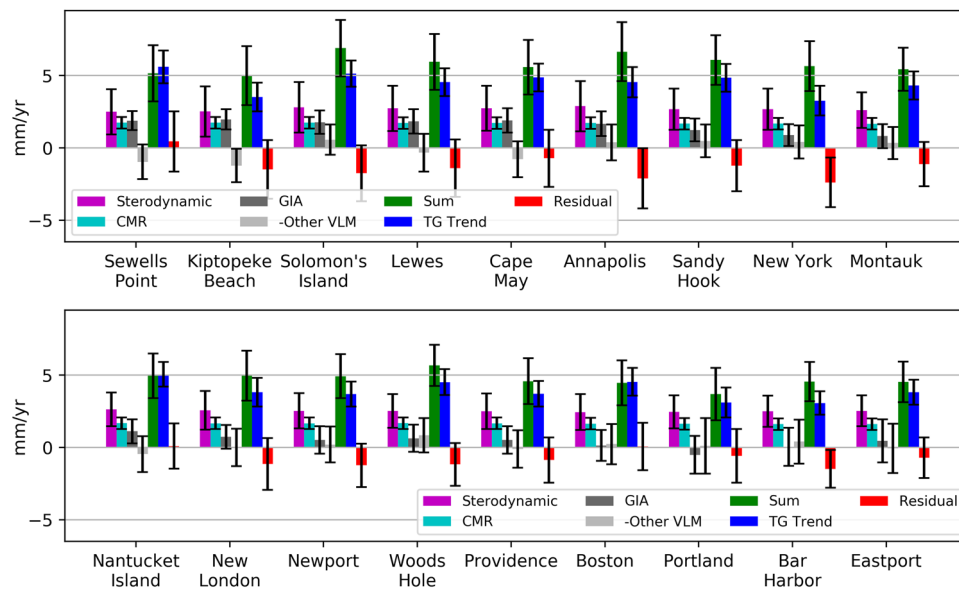
Fig. 4 Northeast sea level trends. Trend assessment from 1993 to 2018 for tide gauges along the U.S. East coast North of Cape Hatteras. Residuals are computed by subtracting the tide-gauge trend from the sum of the contemporary mass redistribution, sterodynamic effects, GIA, and non-GIA vertical land motion components. The vertical land motion component is inverted for interpretability. Uncertainty estimates represent two-standard deviations.

much shorter than the altimeter record[65,66], and most tide gauges do not have a collocated GPS station. To address these limitations, we use a GPS imaging technique[67] to estimate VLM at the tide-gauge location, which involves computing the average of all GPS observations around the tide gauge, and weighting by the record length and distance from the tide gauge (see Methods).

We separate the VLM contributions from GIA from those arising from other processes (Eq. 1). While fully attributing the rate of VLM to particular processes at each tide-gauge location is beyond the scope of this study, it is possible to assess the extent to which VLM may be occurring as a result of local processes. The GIA VLM estimates (GIA_{VLM} in Eqs. 1, 2) at each tide gauge are shown in Fig. 3b, while the GPS-based VLM rates (VLM in Eq. 1) are shown in Fig. 3a. Note that, along the U.S. Atlantic coast, the GIA estimates used here differ from those obtained in other studies (see Fig. S2 for comparison). Since the VLM contribution is tied here solely to the GPS-based estimate (Eq. 1), the choice of GIA model affects the partitioning of VLM into GIA and non-GIA components. Also note that the GIA-induced geoid changes differ among individual estimates. While also absorbing any errors in the chosen GIA model, the differences between the GPS-measured rates and the VLM associated with GIA provides an estimate of the VLM associated with more local processes like groundwater withdrawal and hydrocarbon extraction (Fig. 3c). As an example, there are high rates of non-GIA subsidence along the Gulf Coast, consistent with subsurface fluid extraction that has been ongoing in the area[25]. For more detailed attribution of VLM rates along the east coast in terms of GIA and other processes, the reader is referred to past studies dedicated to this topic (e.g.,[17,18,51]).

Regional sea-level evaluation using tide gauges. We separate the U.S. coastlines into three regions: (1) the northeast coast (the Atlantic coast north of Cape Hatteras), (2) the southeast coast (the Atlantic coast south of Cape Hatteras combined with the Gulf coast), and (3) the west coast (the entire U.S. Pacific coast). This separation follows naturally from the spatial covariance structure of coastal sea-level variability (e.g.,[22,68,69]) and provides a structure for presentation of results.
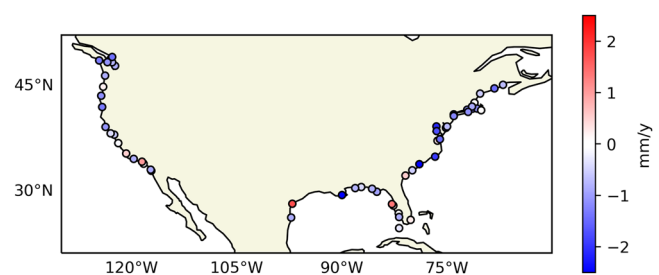

Fig. 5 Trend residuals. Map of the residual sea-level trend estimated as the difference between the combined trend contributions from contemporary mass redistribution, sterodynamic effects, and vertical land motion and the corrected tide-gauge trend following Eq. 1.

The RSL trend assessment for the 18 tide gauges used along the northeast (ordered from south to north) is shown in Fig. 4 (numerical values tabulated in Table S2). The majority of the tide gauges have trends near or above 4 mm/yr. These high rates result in part from GIA-induced subsidence, particularly for mid-Atlantic locations, which is consistent with previous studies in the region[16,18,49]. The GPS-based VLM trends indicate that some locations have higher subsidence rates than predicted by GIA models (e.g., Solomon's Island), suggesting additional VLM not related to GIA[17,70,71]. For 15 of the 18 stations, the residual is not statistically different from zero at the two-standard deviation level. However, Fig. 5 shows that despite the non-significance of their difference from zero, the majority of the residuals are negative, which may point to biases in one or more of the terms on the right-hand side of Eq. 1. The sterodynamic rates in this region have magnitudes around 2.5 mm/y, and do not vary significantly across the region. The coastal sterodynamic trends estimated from ECCO North of Cape Hatteras are higher than in the surrounding areas (Fig. 2b), whereas a similar gradient is not observed in the satellite-altimeter trend pattern (Fig. 1).

Along the Southeast (Fig. 6) 16 out of 17 tide gauges show a trend exceeding 4 mm/yr. The rate associated with contemporary mass redistribution is near the component's global mean of 1.97 mm/yr, while the average contribution from sterodynamic effects approaches 2.5 mm/yr in the region. The large tide-gauge
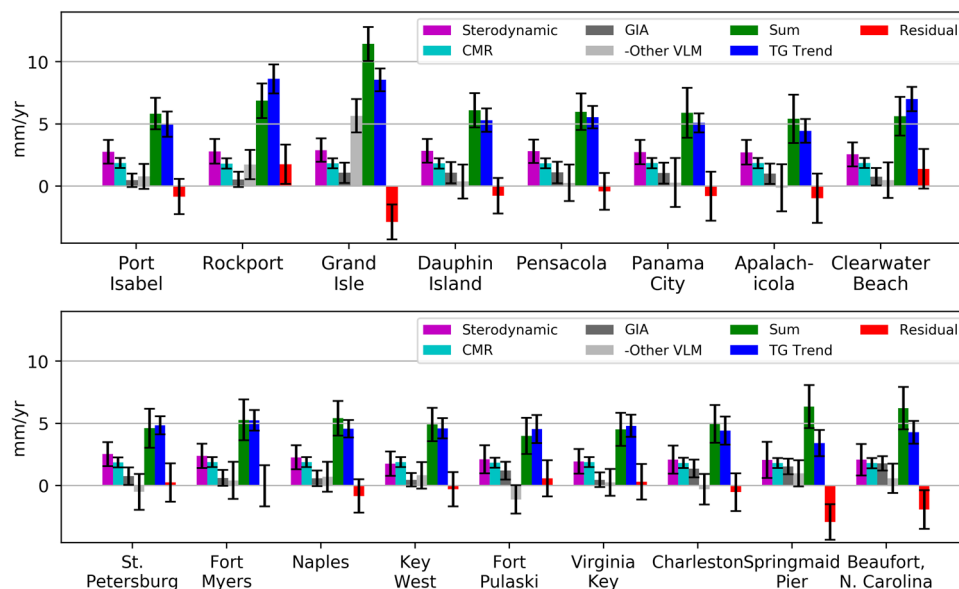
Fig. 6 Southeast and Gulf Coast sea level trends. Trend assessment from 1993 to 2018 for tide gauges along the U.S. southeast and Gulf coasts residuals are computed as the difference between the sum of the contemporary mass redistribution, sterodynamic effects, and GIA, and non-GIA vertical land motion components and the trend measured at the tide gauge. The vertical land motion component is inverted for interpretability. Uncertainty estimates represent two-standard deviations.

trends in Rockport and Grand Isle are tied to residual VLM, associated with subsurface fluid extraction[25]. For the other stations, the residual VLM trend is not significantly different from zero at the two-standard deviation level. In total, 13 of the 17 southeast tide gauges have a RSL residual not statistically different from zero. Similar to the northeast, despite their non-significance the majority of residuals in this region are negative (Fig. 5).

Finally, we consider 20 tide gauges on the west coast (Fig. 7). Consistent with altimetry measurements, the tide-gauge trends are lower than those in the other two regions. Except for the San Diego tide gauge, which is undergoing a high rate of non-GIA subsidence, all of the tide gauges show rates below 3 mm/yr. For the west coast, the sterodynamic contribution is much smaller than the other regions, with rates only slightly above zero. This lower rate over the altimetry era is part of a seesaw pattern in the North Pacific Ocean, and likely caused by internal variability such as the PDO[28]. The lower sterodynamic rate is the primary driver of the lower RSL rates when compared to trends observed in the other regions. In this region, 19 locations have residuals not statistically different from zero, with 4 of these residuals greater than zero. Large positive residuals are found at Santa Monica and Port San Luis, and a large negative residual is estimated at several gauges—mostly concentrated in the Northwest (Fig. 5). These high-magnitude residuals are part of a larger gradient decreasing from south to north along the west coast. RSL trend comparisons on the west coast are more susceptible to uncertainties in GIA and VLM measurements. The model ensemble from Caron et al.[52] shows a large inter-model spread, especially along the Alaskan coastline and around Seattle. Furthermore, GPS stations in this region are generally more sparsely distributed which makes VLM trend estimation with tide gauges more uncertain.

Regional sea-level evaluation using satellite altimetry. Based on comparisons around the U.S. coastlines, we are able to explain RSL trends within the uncertainty estimates at 47 of the 55 tide gauges considered here. This leaves eight locations where trends cannot be explained in terms of the contributing processes. Additionally, even for residuals smaller than our uncertainty

estimates, regional offsets or biases (e.g., northeast region) have been identified that point to potential systematic issues that need further investigation. The satellite-altimetry data provides the opportunity for an additional observation-based assessment. As discussed above, the satellite altimeters measure GSL, which is independent of VLM. As an initial comparison, the altimeter-measured trend at the point nearest the tide gauge is compared to the trend measured at the tide gauge with the VLM trend removed (Fig. 8a). The comparison leads to a substantial spread, particularly for the southeast region where the estimated VLM trends are high.

This evaluation suggests that the VLM estimates are playing a role in driving locations' larger residuals. To investigate this potential disagreement, we evaluate how well the sterodynamic, contemporary mass redistribution, and non-VLM GIA trend contributions explain the altimeter-measured trend (Eq. 3). For the west coast, the sum of the contributions generally agrees with the altimeter trends (Fig. 8b). Examining the distribution of the associated residuals, however, we see that the locations in the northwest have consistently negative residuals. Because of the proximity to the Laurentide Ice Sheet, trends in this region are more susceptible to uncertainties in GIA models, potentially providing an explanation for the negative residuals.

For the northeast, the reconstructed trends from the combined contributions are all higher than the altimeter-measured trends (Fig. 8b). When combined with the negative residuals obtained with the tide gauges (Fig. 5), it appears that the trend contributions from one of the processes is being overestimated in the northeast. While it is difficult to quantitatively assess the source of overestimation, the trends associated with sterodynamic effects in the region are particularly large and likely contributing to the negative biases in this region. Based on the bias present in both this reconstructed sea level comparison with the altimetry and tide gauges, however, it is possible to rule out VLM as the primary contributor the negative offset in the residuals.

For the southeast region, the reconstructed trends generally agree with the trends measured by altimetry, at least relative to the northeast region. As shown in Fig. 5, while there is no coherent bias in the RSL residuals in this region, the
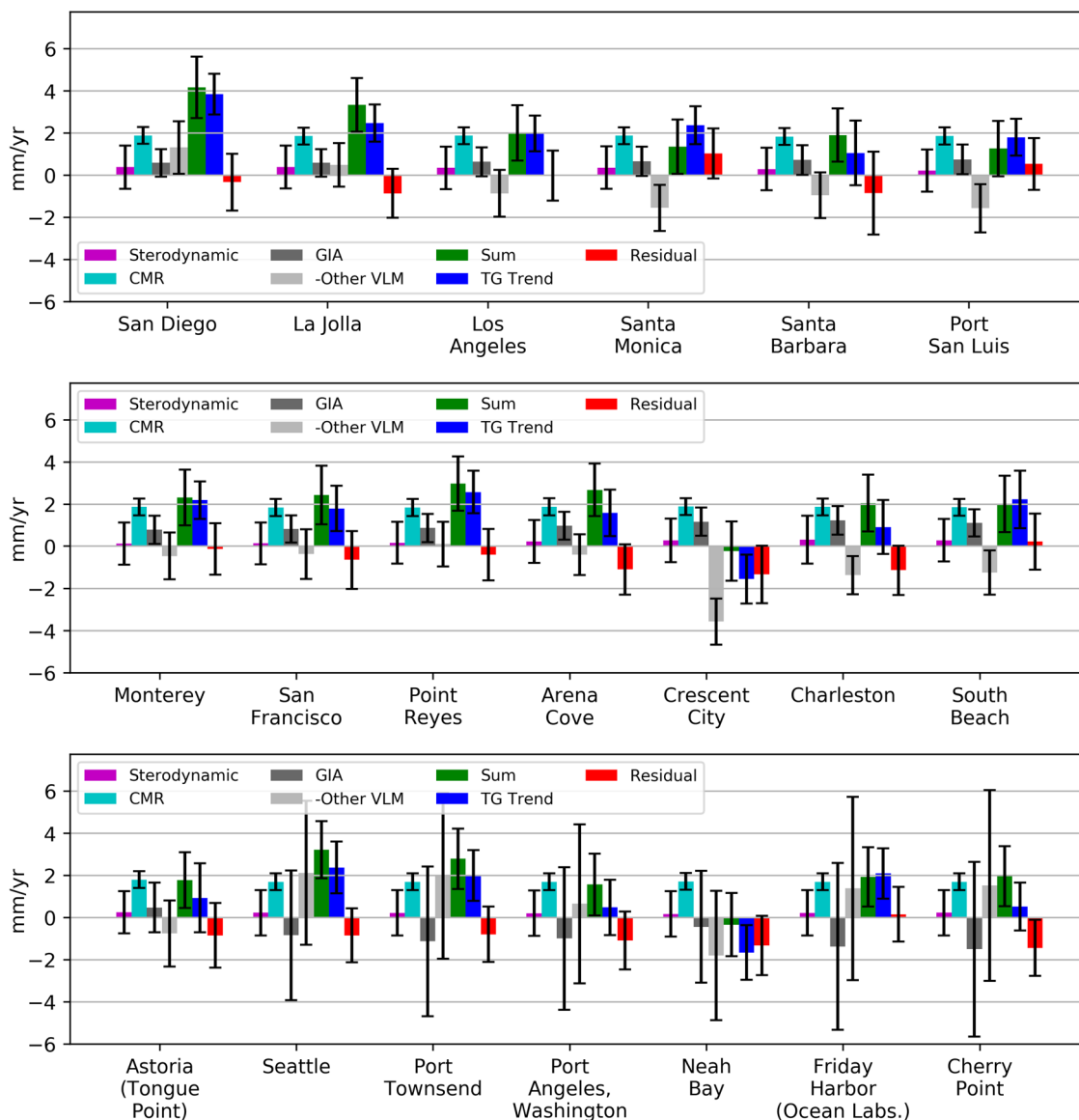
Fig. 7 West Coast sea level trends. Trend assessment from 1993 to 2018 for tide gauges along the U.S. west coast. Residuals are computed as the difference between the sum of the contemporary mass redistribution, sterodynamic effects, and GIA, and non-GIA vertical land motion components and the trend measured at the tide gauge. The vertical land motion component is inverted for interpretability. Uncertainty estimates represent two-standard deviations.

reconstructed GSL residuals with respect to the altimetry trends show a small positive bias (with the exceptions of Rockport and Port Isabel) (Fig. 8d). These results point toward a long-wavelength signal (possibly associated with processes responsible for residuals in the northeast) playing a role in driving a smaller regional bias, and non-GIA VLM driving larger errors on a local scale.

Assessment of vertical land motion estimates. Based on the large spread in Fig. 8a relative to the spread in Fig. 8b, it is likely that the local VLM processes are playing a role in driving the disagreement between the tide-gauge trends and the satellite-altimeter trends for all regions. While GPS observations theoretically capture the relevant VLM processes, the lack of collocated GPS observations, the short and inconsistent time periods of the GPS records, and the presence of discontinuities and low-frequency noise in GPS time series contribute to additional uncertainties that are impossible to quantify. To evaluate the

impact of the lack of collocation, Fig. 9 shows the residuals in Fig. 5 compared to the distance of the tide gauge to the nearest GPS station. There is no clear relationship between the distance from the tide gauge to the nearest GPS station and the magnitude of the residual. Thus, we cannot conclude that a lack of collocation causes larger residuals. Even though a shorter horizontal distance between a tide gauge and GPS receiver should provide a more accurate estimate of VLM experienced by the tide gauge, works such as Keogh and Törnqvist[72] suggest that it does not necessarily guarantee it, for example, when the receiver and tide gauge have foundations at different depths.

Discussion
We have sought to explain and delineate the contributors of the RSL trends observed along the coastlines of the U.S over the time period from 1993 to 2018. Similar investigations have been conducted in other regions and/or other periods[16,18,33,34,73,74], but the entirety of the coastal U.S. provides diversity in terms of
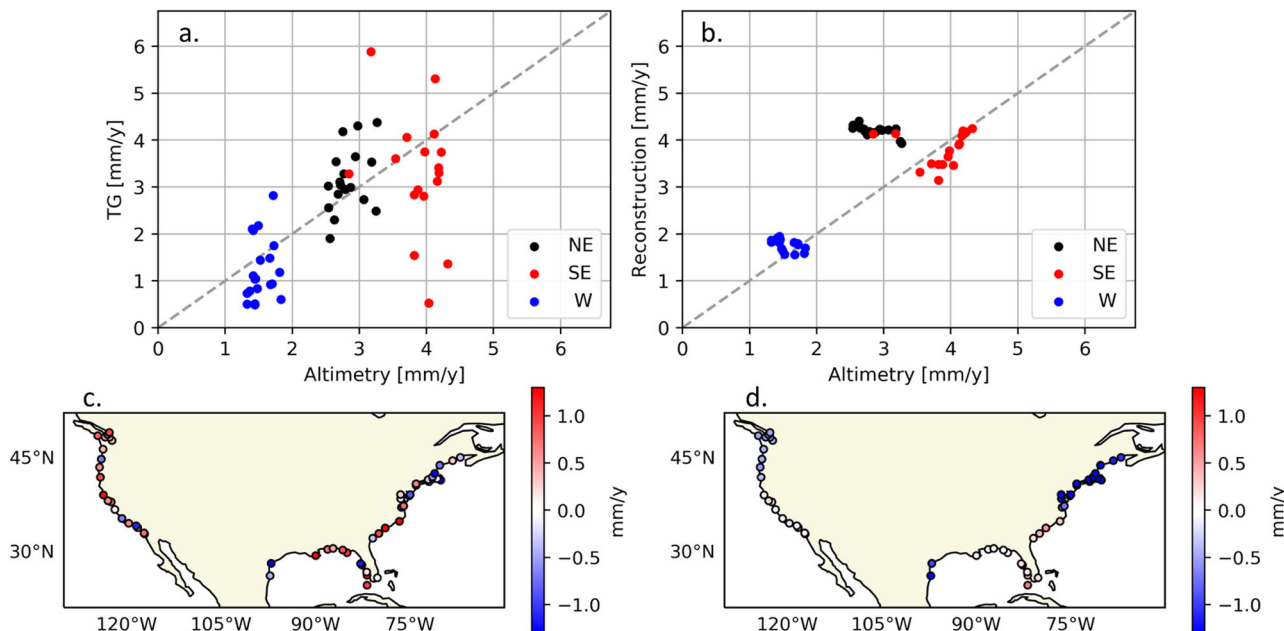
Fig. 8 Assessment of the trends observed by altimetry. a, **c** Comparison with tide-gauge observations (VLM removed). **b**, **d** Comparison with the sum of sterodynamic effects and contemporary mass redistribution and non-VLM GIA.
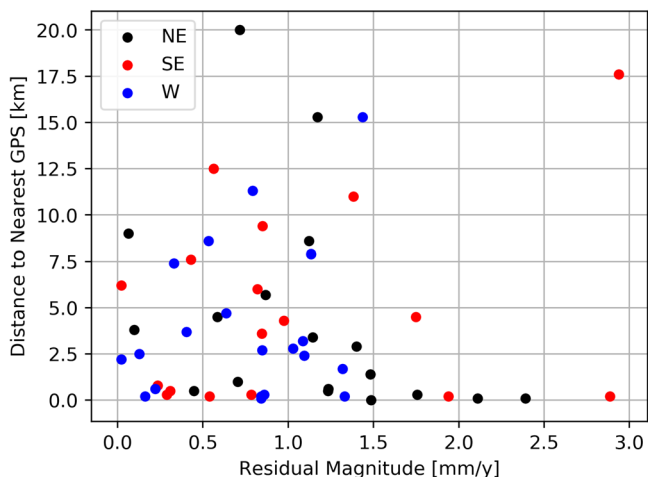

Fig. 9 Evaluation of residuals vs. distance to nearest GPS. Comparison of the magnitudes of the residuals at each tide-gauge location with the distance of the nearest GPS.

the combination of processes affecting regional RSL rise. Additionally, the chosen time period for this investigation offers the opportunity to examine regional RSL change with both in situ measurements and satellite observations.

In 47 of the 55 tide gauges used in this investigation, the difference between the combined estimated contributions from contemporary mass redistribution, sterodynamic effects and VLM is not statistically different at the 95% confidence level from the trends estimated directly from the tide-gauge locations. We do find that there are still multiple sources of uncertainties that hinder the complete attribution of observed sea-level changes to the underlying processes. On larger spatial scales, clear patterns can be seen and explained: observed trends on the west coast are driven primarily by contemporary water mass redistribution and minimally by sterodynamic variability, and many locations around the Gulf coast have experienced particularly high rates of subsidence due to subsurface fluid withdrawal. On the Atlantic

coast, sterodynamic and contemporary mass redistribution rates have similar magnitudes with GIA playing a larger role as tide gauges approach the forebulge to the north.

While the high number of locations with residuals not statistically different from zero demonstrates our ability to account for the trend contributions from the relevant processes, the uncertainty margins are still large, and—especially in the northeast—one or more of the components are possibly biased or not being assessed correctly from our process-based approach. Through additional testing, we have sought to understand the residuals from our analysis and have highlighted both the VLM and sterodynamic trend contributions as likely contributors at locations with larger or regionally biased residuals. Moving forward, assessing the spatial scales of the processes impacting VLM at a particular tide gauge would allow for a determination of how close a GPS station needs to be to account for VLM at the tide-gauge location. A key takeaway, however, is that few of the available tide gauges in the U.S. have a truly collocated GPS station, which would ultimately be a solution to many challenges covered here[75]. Another challenge remains the estimation of sterodynamic effects on coastal sea-level given the limitations of available observations and particular lack of information at the coast. The misfits found in the Northeast region are likely tied to issues with our sterodynamic estimate.

While these needed improvements are generally understood by the scientific community (e.g.,[14,32]), the results contained underscore the importance of maintaining and improving our observing network. As additions to the sea-level observing network are made and available sea-level records continue to lengthen, these gaps in knowledge can be filled and greater confidence can be placed in our understanding of past and ongoing sea-level changes. By demonstrating and communicating a process-based understanding of ongoing RSL rise, increased confidence can be placed in assessments that are used to inform planning efforts. Of additional importance is the knowledge of where uncertainty remains in our understanding of the relevant processes, which can be factored in when planning for future sea-level rise.

Methods

Sea-level observations from tide gauges and altimetry. Monthly tide-gauge records were retrieved from the Permanent Service for Mean Sea-Level[76] (PSMSL, 2019). The global set was first reduced to just those along the coastlines of the contiguous U.S. To ensure the tide gauges considered provide representative data over the time period of interest, records that were less than 70% complete during the time period from 1993 to 2018 were removed. This led to a total of 55 tide gauges along the U.S. coastlines considered in this study (see Table S1). These tide gauges were corrected for the inverse barometer effect using the UK Met Office's HadSLP2 dataset[77] and the inverse barometer relation of Ponte et al.[78]. For altimetry, we use the gridded NASA MEaSUREs Gridded Sea Surface Height Anomalies Version 1812[79]. To compute the altimeter-derived sea-level trend, we take the average trend of all grid cells within a 300 km radius of the tide-gauge location. The 300 km radius was chosen to match the averaging radius used for ECCO data and to maintain enough averaged grid points while capturing local sea-level signals.

Contemporary mass redistribution estimates and glacial isostatic adjustment. Both GIA and contemporary mass redistribution cause gravitational, rotational, and deformation (GRD) effects, which affect tide-gauge, altimetry, and GPS observations. To consistently treat VLM and sea-level observations and since we have separated out the VLM terms in Eqs. 1, 2, we express all changes as GSL changes, and thus only use the geocentric GRD patterns to assess the effects of GIA and contemporary mass redistribution[35,65,80].

We correct all tide-gauge and altimetry observations for the geocentric GRD effects associated with GIA (GIA_{GSL} in Eq. 2) using the estimates from Caron et al.[52] which comes with an estimate of the associated uncertainties.

For the GRD effects from global mass redistribution, we use the estimates from Frederikse et al.[39]. This study provides annual-mean GRD effects resulting from mass changes of ice sheets, glaciers, and land hydrology from groundwater depletion, natural variability, and dam retention. These estimates are based on in situ observations and models for 1993–2003, while for 2003–2019, the estimates are based on GRACE observations[81,82]. Both the in situ and GRACE mass estimates come with an estimate of the uncertainties, based on the individual in situ mass estimate uncertainties and the uncertainties in GRACE processing and GIA, which we propagate into GRD uncertainties. See Frederikse et al.[39] for more details of the computation of these uncertainties.

Sterodynamic sea level. To estimate coastal sterodynamic effects, we use the ECCO state estimate version 4 release 4[83,84]. ECCO is an ocean state estimate, which combines an ocean model with a wide range of observations to compute a physically consistent best estimate of the state of the ocean and provides sterodynamic sea-level changes on an ~1-degree resolution grid. We use the dynamic sea-level variable (SSHDYN) from the model. To avoid the possible influence of small-scale features that lead to trends in single coastal grid cells, we average all ECCO grid points within a 300 km radius around each tide gauge. This 300 km is chosen as a trade-off between having multiple grid cells for each tide gauge and avoiding the inclusion of uncorrelated open-ocean signals.

Since ECCO is constrained to altimetry, the GMSL trend in ECCO does not just represent sterodynamic effects, but also contemporary mass redistribution effects. To avoid double-counting, we remove GMSL from ECCO and add back the observation-based global-mean thermosteric sea-level rise estimate of 1.16 ± 0.4 mm/yr from Cheng et al.[85].

Vertical land motion from GPS observations. To estimate VLM at each tide gauge, we use the GPS imaging method[67], in which all available GPS observations around each tide gauge are averaged, weighted by the distance to the tide gauge and the uncertainty of the VLM trend at the GPS station (see Table S1 for list of GPS stations by tide gauge). We refer to Hammond et al.[67] for a detailed description of the GPS imaging method. All VLM velocities are expressed in the ITRF2014 reference frame[86]. The origin of ITRF2014 tracks the secular changes in the position of the Earth center of mass (CM), which is consistent with our GIA and contemporary GRD estimates.

Linear trend and uncertainty estimation. For the altimetry, tide-gauge, and sterodynamic term, linear trends from 1993 to 2018 were computed via least squares, and the uncertainty was computed as the standard error from the least squares estimate. To account for serial correlation, we reduce the degrees of freedom following the approach of Haigh et al.[87]. The uncertainty on the VLM trend is given by the imaging method. The GIA trend estimates used here contribute additional uncertainty, which is included in the uncertainty estimates.

To estimate uncertainties on the other values in Figs. 4, 6, 7, additional considerations are required. The uncertainties associated with the individual contributors are not strictly independent and must be correctly represented to obtain uncertainties on the combined (sum) contributions and residual terms. Specifically, we use the following equations to estimate the uncertainties on the sum of the contributors and the residual:

$$U_{SUM} = \sqrt{U^2_{CMR,P} + U^2_{SD,P} + U^2_{VLM} + U^2_{GIA} + U^2_{SUM,T}} \qquad (4)$$

$$U_{RES} = \sqrt{U^2_{CMR,P} + U^2_{SD,P} + U^2_{VLM} + U^2_{GIA} + U^2_{RES,T}} \qquad (5)$$

where CMR refers to the contemporary mass redistribution trend, SD is the sterodynamic trend, VLM is the VLM trend, and P and T refer to the process-based uncertainty of data and formal uncertainty from trend estimation (accounting for serial correlation[88]), respectively. $U_{SUM,T}$ and $U_{RESID,T}$ are estimated from the linear trend computation. The process-based uncertainty for contemporary mass redistribution ($U_{CMR,P}$) is computed following Frederikse et al.[39] and is based on the spread among multiple estimates of each individual component (glaciers, ice sheets, and terrestrial water storage), as well as uncertainties in GRACE observations after 2003.

The process-based uncertainty on the sterodynamic trend ($U_{SD,P}$) is provided by the uncertainty in the global-mean thermosteric trend from 1993 to 2018 that is added to the ECCO data (see Sterodynamic section above). Throughout the analysis, all uncertainties are addressed at the 1-sigma level until assessing budget closure and presenting results, at which point we double the values to become a 2-sigma estimate.

Data availability

Tide-gauge data is available from the Permanent Service for Mean Sea Level (https://www.psmsl.org/). GPS data is available from University of Nevada Reno Geodetic Laboratory (http://geodesy.unr.edu/). The ECCO Version 4 Release 4 model output is available from https://ecco.jpl.nasa.gov/drive/files. Gridded Surface Height Anomalies Ver. 1812 available from NASA JPL PO.DAAC, CA, USA at https://doi.org/10.5067/SLREF-CDRV2. The estimates of contemporary mass redistribution and associated GRD patterns are available from https://doi.org/10.5281/zenodo.3862995.

Code availability

Codes for performing the budget calculations and uncertainty estimates are available upon request to B.D.H.

References

1. Church, J. A. & White, N. J. Sea-level rise from the late 19th to the early 21st century. *Surv. Geophys.* **32**, 585–602 (2011).
2. Milne, G. A., Gehrels, W. R., Hughes, C. W. & Tamisiea, M. E. Identifying the causes of sea-level change. *Nat. Geosci.* **2**, 471 (2009).
3. Stammer, D., Cazenave, A., Ponte, R. M. & Tamisiea, M. E. Causes for contemporary regional sea-level changes. *Annu. Rev. Mar. Sci.* **5**, 21–46 (2013).
4. Nicholls, R. J. Planning for the impacts of sea level rise. *Oceanography* **24**, 144–157 (2011).
5. Nicholls, R. J. et al. A global analysis of subsidence, relative sea-level change and coastal flood exposure. *Nat. Clim. Chang.* https://doi.org/10.1038/s41558-021-00993-z (2021).
6. Cazenave, A. & Llovel, W. Contemporary sea-level rise. *Annu. Rev. Mar. Sci.* **2**, 145–173 (2010).
7. Cazenave, A., Palanisamy, H. & Ablain, M. Contemporary sea level changes from satellite altimetry: What have we learned? What are the new challenges? *Adv. Space Res.* **62**, 1639–1653 (2018).
8. Hamlington, B. D., Frederikse, T., Nerem, R. S., Fasullo, J. T., & Adhikari, S. Investigating the acceleration of regional sea-level rise during the satellite altimeter era. *Geophys. Res. Lett.* (2020a).
9. Mazzotti, S., Lambert, A., Van der Kooij, M. & Mainville, A. Impact of anthropogenic subsidence on relative sea-level rise in the Fraser River delta. *Geology* **37**, 771–774 (2009).
10. Nerem, R. S. & Mitchum, G. T. Estimates of vertical crustal motion derived from differences of TOPEX/POSEIDON and tide gauge sea level measurements. *Geophys. Res. Lett.* **29**, 40–1 (2002).
11. Santamaría-Gómez, A. et al. Uncertainty of the 20th century sea-level rise due to vertical land motion errors. *Earth Planet. Sci. Lett.* **473**, 24–32 (2017).
12. Shirzaei, M. & Bürgmann, R. Global climate change and local land subsidence exacerbate inundation risk to the San Francisco Bay Area. *Sci. Adv.* **4**, eaap9234 (2018).
13. Wöppelmann, G. & Marcos, M. Vertical land motion as a key to understanding sea-level change and variability. *Rev. Geophys.* **54**, 64–92 (2016).
14. Hamlington, B. D. et al. Understanding of contemporary regional sea-level change and the implications for the future. *Rev. Geophys.* **58**, e2019RG000672 (2020b).

15. Slangen, A. B. A. et al. A review of recent updates of sea-level projections at global and regional scales. *Surv. Geophys.* **38**, 385–406 (2017).

16. Frederikse, T., Simon, K., Katsman, C. A. & Riva, R. The sea-level budget along the Northwest Atlantic coast: GIA, mass changes, and large-scale ocean dynamics. *J. Geophys. Res. Oceans* **122**, 5486–5501 (2017).

17. Karegar, M. A., Dixon, T. H. & Engelhart, S. E. Subsidence along the Atlantic Coast of North America: Insights from GPS and late Holocene relative sea level data. *Geophys. Res. Lett.* **43**, 3126–3133 (2016).

18. Piecuch, C. G. et al. Origin of spatial variation in US East Coast sea-level trends during 1900–2017. *Nature* **564**, 400–404 (2018a).

19. Domingues, R., Goni, G., Baringer, M. & Volkov, D. What caused the accelerated sea level changes along the US East Coast during 2010–2015? *Geophys. Res. Lett.* **45**, 13–367 (2018).

20. Dong, S., Baringer, M. O. & Goni, G. J. Slow down of the Gulf Stream during 1993–2016. *Sci. Rep.* **9**, 1–10 (2019).

21. Ezer, T. Sea level rise, spatially uneven and temporally unsteady: Why the U.S. East Coast, the global tide gauge record, and the global altimeter data show different trends. *Geophys. Res. Lett.* **40**, 5439–5444 (2013).

22. McCarthy, G. D., Haigh, I. D., Hirschi, J. J. M., Grist, J. P. & Smeed, D. A. Ocean impact on decadal Atlantic climate variability revealed by sea-level observations. *Nature* **521**, 508–510 (2015).

23. Volkov, D. L., Lee, S. K., Domingues, R., Zhang, H. & Goes, M. Interannual sea level variability along the southeastern seaboard of the United States in relation to the gyre-scale heat divergence in the North Atlantic. *Geophys. Res. Lett.* **46**, 7481–7490 (2019).

24. Woodworth, P. L., Maqueda, M. Á. M., Roussenov, V. M., Williams, R. G. & Hughes, C. W. Mean sea-level variability along the northeast A merican A tlantic coast and the roles of the wind and the overturning circulation. *J. Geophys. Res. Oceans* **119**, 8916–8935 (2014).

25. Kolker, A. S., Allison, M. A. & Hameed, S. An evaluation of subsidence rates and sea-level variability in the northern Gulf of Mexico. *Geophys. Res. Lett.* **38**, L21404 (2011).

26. Bromirski, P. D., Miller, A. J., Flick, R. E. & Auad, G. Dynamical suppression of sea-level rise along the Pacific coast of North America: Indications for imminent acceleration. *J. Geophys. Res. Oceans* **116**, C07005 (2011).

27. Piecuch, C. G. et al. How is New England coastal sea level related to the Atlantic meridional overturning circulation at 26° N? *Geophys. Res. Lett.* **46**, 5351–5360 (2019).

28. Hamlington, B. D. et al. Past, present and future pacific sea level-change. *Earths Future* **8**, 2020EF001839, https://doi.org/10.1029/2020EF001839 (2020c).

29. Hamlington, B. D. et al. Uncovering an anthropogenic sea-level rise signal in the Pacific Ocean. *Nat. Clim. Change* **4**, 782–785 (2014).

30. Merrifield, M. A., Thompson, P. R. & Lander, M. Multidecadal sea level anomalies and trends in the western tropical Pacific. *Geophys. Res. Lett.* **39**, L13602 (2012).

31. Moon, J. H., Song, Y. T. & Lee, H. PDO and ENSO modulations intensified decadal sea level variability in the tropical Pacific. *J. Geophys. Res. Oceans* **120**, 8229–8237 (2015).

32. Ponte, R. M. et al. Towards comprehensive observing and modeling systems for monitoring and predicting regional to coastal sea level. *Front. Mar. Sci.* **6**, 437 (2019).

33. Slangen, A. B. A., Van de Wal, R. S. W., Wada, Y. & Vermeersen, L. L. A. Comparing tide gauge observations to regional patterns of sea-level change (1961-2003). *Earth Syst. Dyn.* **5**, 243–255 (2014).

34. Frederikse, T. et al. Closing the sea level budget on a regional scale: trends and variability on the Northwestern European continental shelf. *Geophys. Res. Lett.* **43**, 10–864 (2016).

35. Gregory, J. M. et al. Concepts and terminology for sea level: mean, variability and change, both local and global. *Surv. Geophys.* **40**, 1251–1289 (2019).

36. Farrell, W. E. & Clark, J. A. On postglacial sea-level. *Geophys. J. Int.* **46**, 647–667 (1976).

37. Milne, G. A. & Mitrovica, J. X. Postglacial sea-level change on a rotating Earth. *Geophys. J. Int.* **133**, 1–19 (1998).

38. Mitrovica, J. X., Tamisiea, M. E., Davis, J. L. & Milne, G. A. Recent mass balance of polar ice sheets inferred from patterns of global sea-level change. *Nature* **409**, 1026 (2001).

39. Frederikse, T. et al. The causes of sea-level rise since 1900. *Nature* **584**, 393–397 (2020).

40. Bingham, R. J. & Hughes, C. W. Local diagnostics to estimate density-induced sea level variations over topography and along coastlines. *J. Geophys. Res. Oceans* **117**, C01013 (2012).

41. Vinogradov, S. V. & Ponte, R. M. Low-frequency variability in coastal sea level from tide gauges and altimetry. *J. Geophys. Res. Oceans* **116**, C07006 (2011).

42. Piecuch, C. G. et al. Tide gauge records reveal improved processing of gravity recovery and climate experiment time-variable mass solutions over the coastal ocean. *Geophys. J. Int.* **ume 214**, 1401–1412 (2018b).

43. ECCO Consortium et al. Synopsis of the ECCO Central Production Global Ocean and Sea-Ice State Estimate (Version 4 Release 4). https://doi.org/10.5281/zenodo.3765929 (2020).

44. Wunsch, Carl, Ponte, RuiM. & Heimbach, Patrick Decadal trends in sea level patterns: 1993–2004. *J. Clim.* **20**, 5889–5911 (2007).

45. Piecuch, C. G. & Ponte, R. M. Mechanisms of interannual steric sea level variability. *Geophys. Res. Lett.* **38**, L15605 (2011).

46. Fukumori, I. & Wang, O. Origins of heat and freshwater anomalies underlying regional decadal sea level trends. *Geophys. Res. Lett.* **40**, 563–567 (2013).

47. Brown, S. & Nicholls, R. J. Subsidence and human influences in mega deltas: The case of the Ganges–Brahmaputra–Meghna. *Sci. Total Environ.* **527**, https://doi.org/10.1016/j.scitotenv.2015.04.124 (2015).

48. Milne, Glenn & Mitrovica, Jerry Searching for eustasy in deglacial sea-level histories. *Quat. Sci. Rev.* **27**, 2292–2302 (2008).

49. Davis, J. L. & Mitrovica, J. X. Glacial isostatic adjustment and the anomalous tide gauge record of eastern North America. *Nature* **379**, 331–333 (1996).

50. Engelhart, S. E., Horton, B. P., Douglas, B. C., Peltier, W. R. & Törnqvist, T. E. Spatial variability of late Holocene and 20th century sea-level rise along the Atlantic coast of the United States. *Geology* **37**, 1115–1118 (2009).

51. Engelhart, S. E. & Horton, B. P. Holocene sea level database for the Atlantic coast of the United States. *Quat. Sci. Rev.* **54**, 12–25 (2012).

52. Caron, L. et al. GIA model statistics for GRACE hydrology, cryosphere, and ocean science. *Geophys. Res. Lett.* **45**, 2203–2212 (2018).

53. Burgette, R. J., Weldon, R. J. II & Schmidt, D. A. Interseismic uplift rates for western Oregon and along-strike variation in locking on the Cascadia subduction zone. *J. Geophys. Res.* **114**, B01408 (2009).

54. Bekaert, D. P. S., Hamlington, B. D., Buzzanga, B. & Jones, C. E. Spaceborne synthetic aperture radar survey of subsidence in Hampton Roads, Virginia (USA). *Sci. Rep.* **7**, 1–9 (2017).

55. Jones, C. E. et al. Anthropogenic and geologic influences on subsidence in the vicinity of New Orleans, Louisiana. *J. Geophys. Res. Solid Earth* **121**, 3867–3887 (2016).

56. Ojha, C., Shirzaei, M., Werth, S., Argus, D. F. & Farr, T. G. Sustained groundwater loss in California's Central Valley exacerbated by intense drought periods. *Water Resour. Res.* **54**, 4449–4460 (2018).

57. Dixon, T. H. et al. Subsidence and flooding in New Orleans. *Nature* **441**, 587–588 (2006).

58. Meckel, T. A., ten Brink, U. S. & Williams, S. J. Current subsidence rates due to compaction of Holocene sediments in southern Louisiana. *Geophys. Res. Lett.* **33**, L11403 (2006).

59. Nicholls, R. J. & Cazenave, A. Sea-level rise and its impact on coastal zones. *Science* **328**, 1517–1520 (2010).

60. Miller, M. M. & Shirzaei, M. Land subsidence in Houston correlated with flooding from Hurricane Harvey. *Remote Sens. Environ.* **225**, 368–378 (2019).

61. Johnson, C. S. et al. The role of sediment compaction and groundwater withdrawal in local sea-level rise, Sandy Hook, New Jersey, USA. *Quat. Sci. Rev.* **181**, 30–42 (2018).

62. Hamlington, B. D. et al. An ongoing shift in Pacific Ocean sea level. *J. Geophys. Res. Oceans* **121**, 5084–5097 (2016).

63. Dangendorf, S. et al. Reassessment of 20th century global mean sea level rise. *Proc. Natl Acad. Sci.* **114**, 5946–5951 (2017).

64. Kleinherenbrink, M., Riva, R. & Frederikse, T. A comparison of methods to estimate vertical land motion trends from GNSS and altimetry at tide gauge stations. *Ocean Sci.* **14**, 187–204 (2018).

65. Frederikse, T., Landerer, F. W. & Caron, L. The imprints of contemporary mass redistribution on local sea level and vertical land motion observations. *Solid Earth* **10**, 1971–1987 (2019).

66. Santamaría-Gómez, A. & Mémin, A. Geodetic secular velocity errors due to interannual surface loading deformation. *Geophys. J. Int.* **202**, 763–767 (2015).

67. Hammond, W. C., Blewitt, G. & Kreemer, C. GPS Imaging of vertical land motion in California and Nevada: Implications for Sierra Nevada uplift. *J. Geophys. Res. Solid Earth* **121**, 7681–7703 (2016).

68. Thompson, P. R. & Mitchum, G. T. Coherent sea level variability on the North Atlantic western boundary. *J. Geophys. Res. Oceans* **119**, 5676–5689 (2014).

69. Calafat, F. M., Wahl, T., Lindsten, F., Williams, J. & Frajka-Williams, E. Coherent modulation of the sea-level annual cycle in the United States by Atlantic Rossby waves. *Nat. Commun.* **9**, 1–13 (2018).

70. Kopp, R. E. Does the mid-Atlantic United States sea level acceleration hot spot reflect ocean dynamic variability? *Geophys. Res. Lett.* **40**, 3981–3985 (2013).

71. Miller, K. G., Kopp, R. E., Horton, B. P., Browning, J. V. & Kemp, A. C. A geological perspective on sea-level rise and its impacts along the US mid-Atlantic coast. *Earths Fut.* **1**, 3–18 (2013).

72. Keogh, M. E. & Törnqvist, T. E. Measuring rates of present-day relative sea-level rise in low-elevation coastal zones: a critical evaluation. *Ocean Sci.* **15**, 61–73 (2019).

73. Richter, K., Nilsen, J. Ø. & Drange, H. Contributions to sea level variability along the Norwegian coast for 1960–2010. *J. Geophys. Res. Oceans* **117** (2012).

74. Rietbroek, R., Brunnabend, S. E., Kusche, J., Schröter, J. & Dahle, C. Revisiting the contemporary sea-level budget on global and regional scales. *Proc. Natl Acad. Sci.* **113**, 1504–1509 (2016).
75. Woodworth, P. L., Wöppelmann, G., Marcos, M., Gravelle, M. & Bingley, R. M. Why we must tie satellite positioning to tide gauge data. *Eos* **98**, https://doi.org/10.1029/2017EO064037 (2017).
76. Holgate, S. J. et al. New data systems and products at the permanent service for mean sea level. *J. Coast. Res.* **29**, 493–504 (2013).
77. Allan, R. & Ansell, T. A new globally complete monthly historical gridded mean sea level pressure dataset (HadSLP2): 1850–2004. *J. Clim.* **19**, 5816–5842 (2006).
78. Ponte, R. M. Low-frequency sea level variability and the inverted barometer effect. *J. Atmos. Ocean. Technol.* **23**, 619–629 (2006).
79. Zlotnicki, V., Qu, Z., Willis, J. K, Ray, R. & Hausman, J. *MEaSUREs Gridded Sea Surface Height Anomalies Version 1812*, https://doi.org/10.5067/SLREF-CDRV2 (2019).
80. Tamisiea, M. E. & Mitrovica, J. X. The moving boundaries of sea level change: understanding the origins of geographic variability. *Oceanography* **24**, 24–39 (2011).
81. Watkins, M. M., Wiese, D. N., Yuan, D. N., Boening, C. & Landerer, F. W. Improved methods for observing Earth's time variable mass distribution with GRACE using spherical cap mascons. *J. Geophys. Res. Solid Earth* **120**, 2648–2671 (2015).
82. Wiese, D. N., Landerer, F. W. & Watkins, M. M. Quantifying and reducing leakage errors in the JPL RL05M GRACE mascon solution. *Water Resour. Res.* **52**, 7490–7502 (2016).
83. Forget, G. A. E. L., Campin, J. M., Heimbach, P., Hill, C. N., Ponte, R. M. & Wunsch, C. ECCO version 4: An integrated framework for non-linear inverse modeling and global ocean state estimation. *Geoscientific Model Development* **8**, 3071–3104 (2015).
84. Fukumori, I. et al. Data sets used in ECCO Version 4 Release 3, http://hdl.handle.net/1721.1/120472 (2018).
85. Cheng, L. et al. Improved estimates of ocean heat content from 1960 to 2015. *Sci. Adv.* **3**, e1601545 (2017).
86. Altamimi, Z., Rebischung, P., Métivier, L. & Collilieux, X. ITRF2014: a new release of the International Terrestrial Reference Frame modeling nonlinear station motions. *J. Geophys. Res. Solid Earth* **121**, 6109–6131 (2016).
87. Haigh, I. D. et al. Timescales for detecting a significant acceleration in sea level rise. *Nat. Commun.* **5**, 1–11 (2014).
88. Royston, S. et al. Sea-level trend uncertainty with Pacific climatic variability and temporally-correlated noise. *J. Geophys. Res. Oceans* **123**, 1978–1993 (2018).

Author contributions
T.C.H. and B.D.H. conceived of the experiment, performed the core analysis, interpretation of results, and writing. C.G.P., T.F., and R.E.K. assisted in conceiving of the experiment, provided data for the analysis, interpreting the results, and assisted in writing the paper. W.C.H., G.B., I.F., and J.S.W. provided data for the analysis, assisted in interpretation of results, and writing of the paper. P.R.T., R.S.N., J.T.R., F.W.L., D.P.S.B., H.C., D.T., and C.B. assisted in interpretation of results and writing the paper.

Competing interests
The authors declare no competing interests.

Additional information
Supplementary information The online version contains supplementary material available at https://doi.org/10.1038/s43247-021-00300-w.

Correspondence and requests for materials should be addressed to B. D. Hamlington.

Peer review information *Communications Earth & Environment* thanks the anonymous reviewers for their contribution to the peer review of this work. Primary Handling Editor: Heike Langenberg

Reprints and permission information is available at http://www.nature.com/reprints

Publisher's note Springer Nature remains neutral with regard to jurisdictional claims in published maps and institutional affiliations.